ORIGINAL RESEARCH

Ultrastructure of Bone: Hierarchical Features from Nanometer to Micrometer Scale Revealed in Focused Ion Beam Sections in the TEM

Kathryn Grandfield[1,2] · Vicky Vuong[1] · Henry P. Schwarcz[2,3]

Abstract

The ultrastructure of bone has been widely debated, in part due to limitations in visualizing nanostructural features over relevant micrometer length scales. Here, we employ the high resolving power and compositional contrast of high-angle annular dark-field scanning transmission electron microscopy (HAADF STEM) to investigate new features in human bone with nanometer resolution over microscale areas. Using focused ion beam (FIB)-milled sections that span an area of 50 μm^2, we have shown how most of the mineral of cortical human osteonal bone occurs in the form of long, thin polycrystalline plates (mineral lamellae, MLs) which are either flat or curved to wrap closely around collagen fibrils. Close to the collagen fibril (< 20 nm), the radius of curvature matches that of the fibril diameter, while at greater distances, MLs form arcs with much larger radii of curvature. In addition, stacks of closely packed planar (uncurved) MLs occur between fibrils. The curving of mineral lamellae both around and between the fibrils would contribute to the strength of bone. At a larger scale, rosette-like clusters of fibrils are noted for the first time, arranged in quasi-circular arrays that define tube-like structures in alternating osteonal lamellae. At the boundary between adjacent osteonal lamellae, the orientation of fibrils and surrounding mineral lamellae changes abruptly, resembling the "orthogonal" patterns identified by others (Reznikov et al. in Acta Biomater 10:3815–3826, 2014). These features spanning nanometer to micrometer scale have implications for our understanding of bone structure and mechanical integrity.

✉ Kathryn Grandfield
kgrandfield@mcmaster.ca

✉ Henry P. Schwarcz
schwarcz@mcmaster.ca

1 Department of Materials Science and Engineering, McMaster University, 1280 Main St W, ETB 403, Hamilton, ON L8S 4L7, Canada

2 School of Biomedical Engineering, McMaster University, Hamilton, ON L8S 4L7, Canada

3 School of Geography and Earth Sciences, McMaster University, Hamilton, ON L8S 4L7, Canada

Introduction

Bone is a composite material in which a scaffold of collagen fibrils is associated with approximately equal volumes of apatite mineral. The collagen occurs in the form of fibrils in which molecules of collagen are arranged in a staggered array; 40-nm-long gaps which occur between the ends of collinear molecules are arranged in zones that span the width of the fibrils. The gap zones are spaced 67 nm apart [1]. The mineral occurs in the form of plates some 20–50 nm wide as shown by small-angle X-ray scattering (SAXS) [2] and direct imaging of crystals extracted from bone by digestion in bleach (NaClO) [3] or hydrazine [4].

A general consensus has existed for many years among bone researchers that most of the mineral in bone resides in the gap zones [5–7]. Some authors propose that mineral extends continuously between adjacent gaps [8], while other authors, noting the ~50 volume percent mineral fraction of bone cannot fit in the gap zones, suggest that mineral extends

into the adjacent 27-nm-long overlap zones [9]. Other writers have proposed that some or most of the mineral lies outside the fibrils [10] although the detailed nature of the extrafibrillar mineral was not specified.

Recently, using broad-beam ion milling methods for sectioning bone, it has been shown that most of the mineral in bone occurs in the form of elongated polycrystalline plates which are uniformly about 5 nm thick, up to 200 nm long, and at least 60–80 nm wide. These plates appeared to be either curved around the collagen fibrils or organized in stacks of planar sheets [11].

The thin, polycrystalline plates which we observe resemble in some dimensional respects "platelets" which have been identified in bone using small-angle X-ray scattering methods (SAXS) [12, 13]. However, we will refer to the structures which we have observed in TEM images as "mineral lamellae" (MLs) [14, 15]. It is likely that the platelets identified by SAXS, which have dimensions of about 2–7 nm and lengths of approximately 15–200 nm [12], are in fact MLs. However, SAXS does not provide information about the internal characteristics or the curvature of the plates as is directly visualized from TEM images. SAXS uses the broadening of the primary X-ray beam which is insensitive to strain or crystal imperfections but depends exclusively on the outer dimensions of the crystals. It is used to determine size, orientation, and spatial arrangement of 0.5–50 nm particles over microscale volumes [2]. Whereas TEM provides a direct measure of the structure with high spatial resolution, but is often limited in sampling volume. In this manuscript, we use TEM imaging to analyze these MLs in mature, osteonal, lamellar bone.

Many of the TEM images on which traditional bone ultrastructure models have been based were carried out on ultramicrotomed sections [5, 7–9, 16]. Previous studies comparing TEM images of ultramicrotomed and ion-milled samples of the same bone (Fig. 10 in McNally et al., and Fig. 4 in Jantou et al.) have concluded that the diamond blade of the ultramicrotome shatters the elongated mineral structures (mineral lamellae) which are clearly revealed in ion-milled sections of bone. Therefore, it was previously impossible to recognize many of the nm-scale structural features in bone which have become apparent in ion-milled sections. However, most previous studies of ion-milled bone [11, 14, 15] have been limited to studying a zone about 400 nm wide surrounding holes produced during ion milling. Focused ion beam (FIB) milling of sections cut from polished blocks of bone permits us to produce sections up to several tens of μm^2 in area [17]. This method has been demonstrated on elephant ivory [18], human bone [19], and applied widely in human-bone implant studies [20, 21]. By producing large FIB-milled sections, and investigating them by TEM, we are able to visualize features in the ultrastructure of bone which were not previously discernable. To some extent,

these bridge the gap between our previous studies at the nanometer scale, with studies of demineralized bone at the micrometer scale performed by others [22]. In particular, we can now begin to see the relation of the mineralized ultrastructure to the higher hierarchical level of the osteonal lamellae and examine the validity of the "twisted plywood" model for bone [23].

## Materials and Methods

Sample Preparation

The present study was carried out on a piece of cortical bone from the femur of a healthy, 19-year-old male; the sample was obtained with ethical approval as a by-product of restorative surgery. A section approximately 2 cm × 2 cm × 1.3 cm, containing both cortical and trabecular bone was fixed after retrieval with formalin, and then stained with 1% osmium tetroxide. In a previous study, we showed there was no difference in the appearance in TEM images of a sample of bovid bone which had been treated with formalin and osmium tetroxide compared to an untreated sample [11]. Osmium generally stains the protein (collagen) and spectroscopic data have shown that MLs are indeed Ca and P containing, and not osmium. Only cortical bone was examined in this study. The sample was progressively dehydrated through a series of increasing ethanol concentrations (50, 70, 95, 95, 100%), then further dehydrated in a critical point dryer at 40 °C. A block was cut from the cortical bone using a diamond-edged slow-speed saw; the long axis of the block was oriented parallel to the long axis of the femur (Fig. 1).

Focused Ion Beam Milling

Samples for transmission electron microscopy (TEM) were prepared from the bone sample using conventional FIB-SEM in situ lift-out procedures (Fig. 2). To reduce charging, the sample was sputter-coated for 60 s with gold. The TEM sections were prepared using a Zeiss NVision 40 (Carl Zeiss AG, Germany) FIB-SEM equipped with a 30 kV gallium ion column, carbon gas injector system, and Kleindiek probe drive system.

Sections were cut in two orientations: parallel (longitudinal) to the orientation of the long axis of the bone ("parallel section"); and perpendicular or transverse to the long axis ("perpendicular section"). A single parallel section was prepared, which appears to lie within one osteonal lamella marked in Fig. 2. Shallow grooves on the surface of the sample were oriented parallel to the long axis of the bone. We infer that these are the boundaries between osteonal lamellae [23]. Two perpendicular sections were prepared to test the homogeneity of the sample (Fig. 2 shows one of these).

Fig. 1 Schematic highlighting the regions of interest from the human femur and sites selected for TEM sample preparation by FIB. The center image shows how FIB was used to lift-out sections parallel and perpendicular to the long axis of the femur, and the resulting microstructure in the STEM HAADF
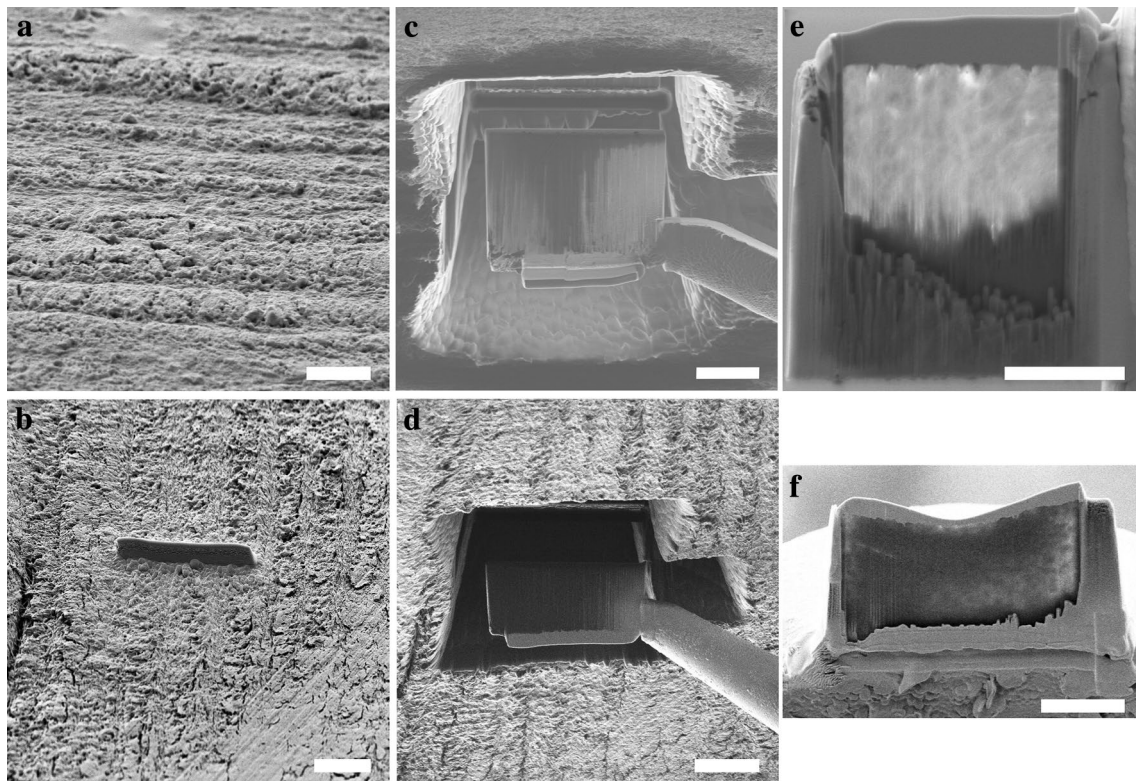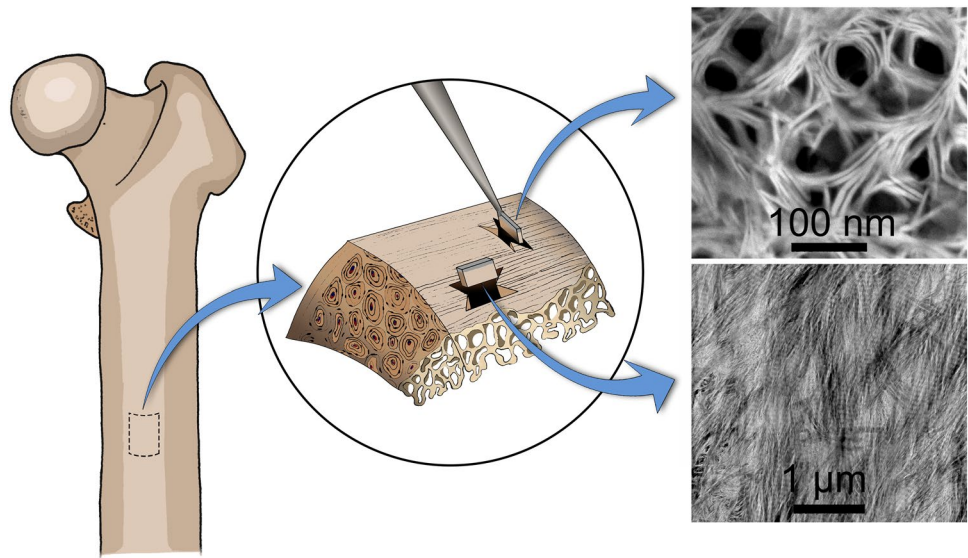
Fig. 2 Focused ion beam sample preparation. SEM images of the bone block during FIB preparation for parallel (top row) and perpendicular (bottom row) sections. **a, d** Region of interest and carbon deposition. **b, e** Rough milling and lift-out by micromanipulator. **c, f** Lamella attached to a TEM grid and final thinning to electron transparency. Scale bars 6 μm

Transmission Electron Microscopy

A Titan 80–300 microscope (FEI Company, The Netherlands) was operated at 300 keV in high-angle annular dark-field scanning transmission electron microscopy (HAADF STEM) mode for imaging. Intensity in the HAADF images is approximately proportional to Z^2 ($Z =$ atomic number); high-Z regions appear bright, while regions with little or no matter in them are dark.

Multiple HAADF-STEM images were obtained at magnifications of 20 and 57 kX, covering essentially the total area of each FIB section. Each individual image is 1.1×1.1 µm. These images were then assembled into composite images (mosaics) using Microsoft Image Composite Editor (Microsoft Corporation, USA) software. The mosaics extend over areas ranging from 30 to 160 µm^2.

Electron tomography on the perpendicular section was performed over $\pm 60°$. The sample was mounted in the Model 2020 Advanced Tomography Holder (E.A. Fischione Instruments, Inc., Export, PA), images were recorded every $2°$ in HAADF STEM with the automated focusing, image shifting, and acquisition of the Inspect 3D software (FEI Company, The Netherlands). The full tilt-series collected is visible in the supplemental information.

Image Analysis

Measurements of dimensions of features (thickness of mineral lamellae, etc.) were made using two methods: (a) Adobe Photoshop, Version 12.0×64, using the ruler tool in the Analysis set; (b) using various tools in Fiji, a version of ImageJ developed by the National Institutes of Health, USA [24]. The tools will be described where the data are presented.

Results

Parallel Section

A section oriented parallel to the long axis of the bone was imaged. Individual 1.1×1.1 µm HAADF-STEM images were assembled into a mosaic covering an area of about 34 µm^2 (Fig. 3). The mosaic is a rectangle whose longer dimension is parallel to the long axis of the bone.

Fibrils and mineral lamellae lie in the plane of this section which was cut parallel to the long axis of the bone.
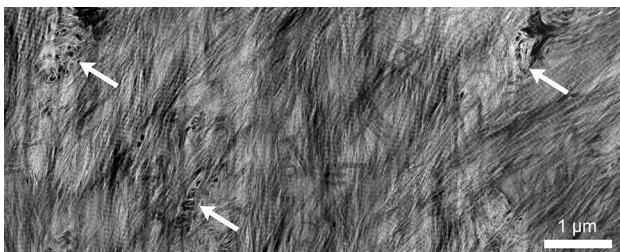
Fig. 3 Composite HAADF-STEM image of the parallel FIB section. Collagen fibrils are oriented normal to 67-nm space banding which is visible across entire image; fibrils and MLs (bright contrast) oriented parallel to collagen fibrils gradually change in orientation across the entire image. Three disordered zones with differing collagen fibril arrangement are marked with arrows; scale bar = 1 µm

We do not see cross-sections of fibrils in sections with this orientation. This is consistent with the fact that fibrils in the cortical bone of long bones are uniformly oriented within curved planar sheets (osteonal lamellae) that wrap around osteons, whose axes are themselves approximately parallel to the bone axis, consistent with commonly held descriptions of the hierarchical structure of bone (e.g., [25]).

Collagen fibrils are identifiable in the mosaic by the presence of gap (dark) and overlap (light) zone couplets repeated along the lengths of the fibrils. The average width of the gap zones is 36.7 ± 3.3 nm ($n = 20$); the repeat (D) length is 67 ± 3 nm. Electron contrast in the gap zone is due to presence of a Ca-P mineral [18]. The mosaic allows us to see that the gap/overlap zones extend in perfect registry between adjacent fibrils, over distances of up to 2.5 µm as previously noted by [22] who also showed that this pattern existed in three dimensions. The extended registry of these couplets implies that at the time of formation of the osteoid parent of the bone, these zones were contiguous and in held in registry as a result of bonding between adjacent fibrils facilitated by extrafibrillar molecules [26, 27].

Using image analysis software (directionality plugin, Fiji [24]), the average orientation of the fibrils and their associated MLs were determined to be $63°$ away from the horizontal base of the image. Since the base is approximately parallel to the long axis of the bone, therefore the orientation of the fibrils + MLs is almost orthogonal to the long axis of the bone; in [28] this orientation is referred to as "low angle." Supplementary Fig. S1 shows a histogram of these angles. While the Fiji tool does not specify precisely what features were detected by the directionality plugin, it seems likely that the analysis captures the orientations of the prominent high-contrast MLs. The histogram would therefore also represent the orientations of collagen fibrils, since these are known to be oriented parallel to MLs. There is no peak at $\sim 30°$ which would represent the orientation of the lines of gap and overlap zones in registry between adjacent fibrils. The histogram can be fitted by a normal distribution, with $r^2 = 0.98$.

The mosaic of the parallel section resembles in some respects, one of the single frames in the serial sections of demineralized bone shown by Reznikov et al. [22]. These authors investigated SEM images of demineralized bone in which the collagen had been stained to improve contrast. The contrast in our images is generated instead by the mineral, showing that it conforms closely to the pattern of the fibrils and, as seen more clearly in our single higher-resolution views, the mineral occurs mainly in the form of elongated mineral lamellae between these fibrils.

Disordered zones in which small groups of fibrils extend for a few µm have been described in bone [28]. We see regions in the parallel section (Fig. 3) which could represent such disordered zones. These occupy about

5% of the total volume of the bone, which appears to be considerably less than the fraction shown in figures from [28]. Some regions (Fig. 4a) resemble typical views of the perpendicular section presented next; the boundary between these regions and adjacent normal fibrils is very sharp and appears to show a flip in orientation of fibrils to one approximately perpendicular to the orientation of the remainder of the parallel section. Other disordered regions consist of areas a few μm² in area in which mineralized features appear to swirl about in a chaotic manner (Fig. 4b). No collagen banding appears to be present in these areas. Due to their near spherical nature, it is also plausible that these regions represent areas near the lacunar-canalicular network (LCN) of bone, which has been shown in FIB-SEM 3D imaging only to appear as electron-dense rimmed voids similar in shape and size [29].
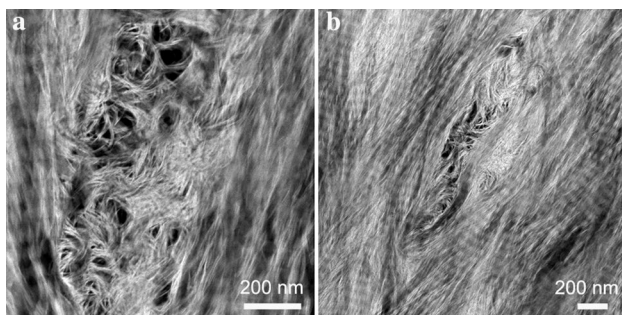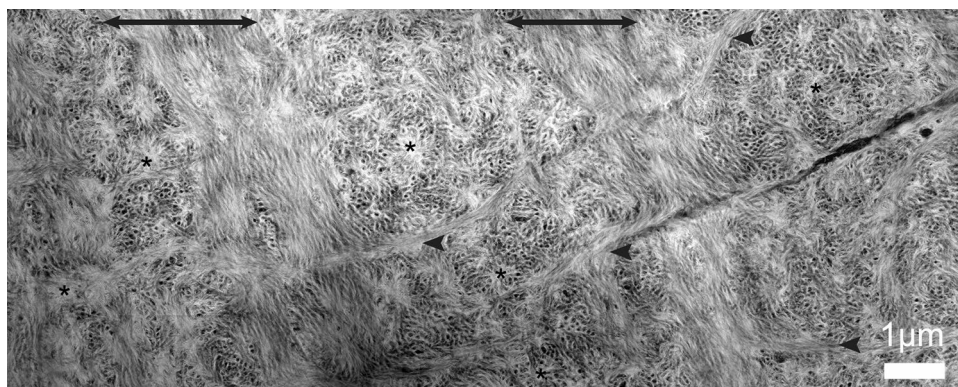
Perpendicular Sections

In contrast to the parallel mosaic, the perpendicular mosaic (Fig. 5) crosses several osteonal lamellae, and is traversed by bands of differing organization; two of them (marked by double ended arrows) closely resemble the collagen fibril and MLs structure seen in the parallel section. In the intermediate sections, we see circular features that closely resemble those shown in previous studies using bright-field images of ion-milled sections [11], including circular "holes" marking position of ~50-nm-diameter collagen fibrils, surrounded by stacks of mineral lamellae. Other previously unrecognized features include the curvature of mineral lamellae, features that resemble "rosettes," marked by asterisks, and details about the orientation between osteonal lamellae; these are discussed in detail below.

Curvature of Mineral Lamellae

In our previous studies of bone, we observed that, when viewed in cross-section, some mineral lamellae appear to wrap around the fibrils. This pattern led us to construct a model (Fig. 6d) in which the polycrystalline plates of the mineral lamellae occur either curved into hemi-cylindrical forms with radii of curvature comparable to the radius of the adjacent fibril, or as flat plates stacked between the fibrils.

The high-resolution HAADF-STEM images, with improved Z-contrast to TEM, clearly confirm this model (Fig. 6b, c). Slightly lower magnification HAADF-STEM images (Fig. 8) now reveal that a curved form is also present in MLs not close to the fibrils. Curved MLs extend over almost the entire volume of bone. Figure 8 shows this pattern at an intermediate scale where we have highlighted some of the curved plates that are not close to fibrils with dotted lines. They approximate cylindrically curved sheets and

Fig. 4 Higher magnification HAADF-STEM images of disordered zones in the parallel section. **a** Oval-shaped patches resembling views of perpendicular section. **b** More chaotic organization of mineralized fibrils; scale bar = 200 nm

Fig. 5 Composite HAADF-STEM images of the perpendicular (transverse) FIB section. Double-headed arrows mark osteonal lamellae with fibrils in parallel or planar orientation, which are flanked by regions with collagen fibrils oriented roughly perpendicularly. Dark spots ("holes") 50 nm in diameter mark positions of collagen fibrils in cross-section (see Fig. 6 for detailed view). Rosette-like features are marked by asterisks. Arrowheads indicate connections between lamellae, which may be a part of the LCN; scale bar = 1 μm

Fig. 6 Detailed features from the perpendicular section. **a** Close-up of a rosette showing swirling mineral lamellae at the center. **b** Stacks of MLs wrapping around single collagen fibrils. **c** Single MLs passing through the interior of fibrils (white arrows). **d** Model of ultrastructure of bone. Orange: mineral lamellae, wrapping around fibrils. Red arrow: stack of mineral lamellae between two fibrils. White arrow: collagen fibril (dark gray = gap zone); scale = 100 nm. (Color figure online)
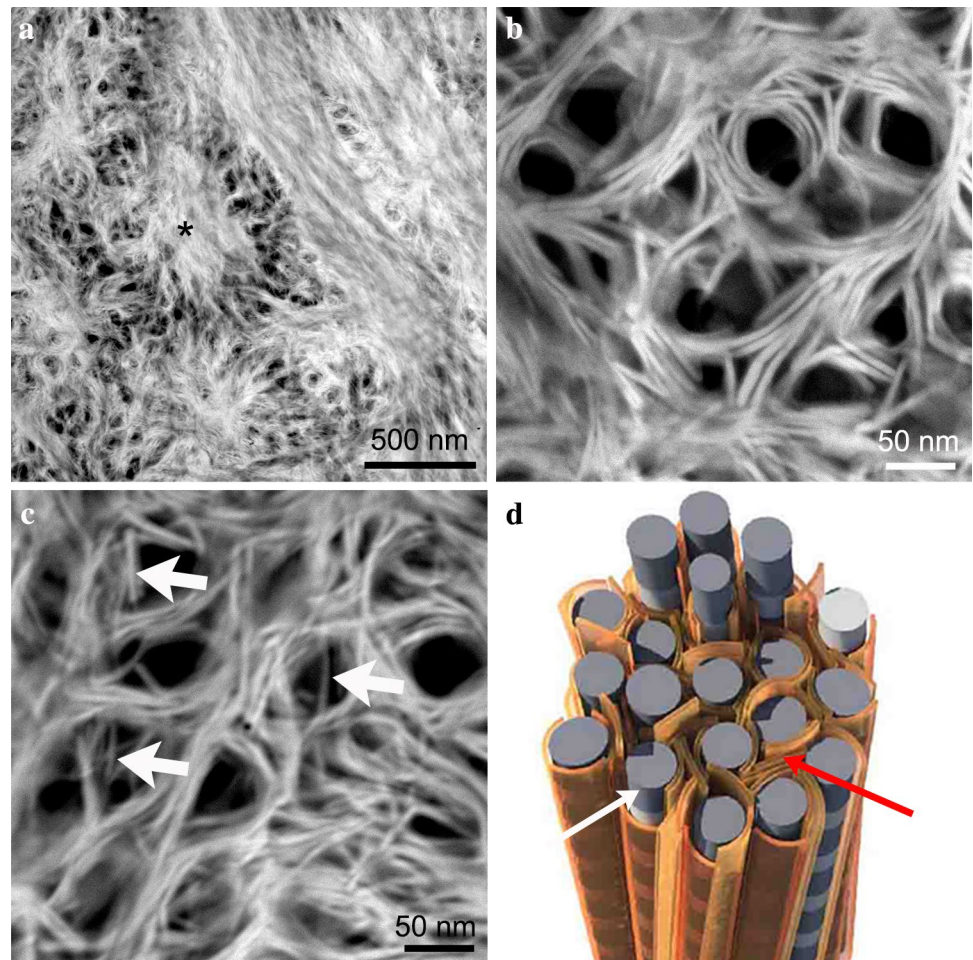
allow us to measure the radii of curvature; the average radius is 79 ± 15 nm. In contrast, the average radius of curvature of the plates immediately surrounding the fibrils marked by arrowheads is 20 ± 4 nm (that is, the average diameter of the fibrils is 44 ± 8 nm). The distribution of radii of curvature of MLs appears to be bimodal, with very few radii > 100 nm, but with a significant number of apparently uncurved MLs (i.e., with infinite radius), which comprise stacks that are also a significant feature of the bone ultrastructure.

We infer that the curved MLs with large radii are actually larger-scale curved plates, shown schematically in Fig. S3. In the figure, we suggest that the plates are curved so that the axes of their cylindrical forms are approximately parallel to the fibril axes. These plates would presumably also extend for some tens of nm in the direction normal to the plane of the section. Lengths measured *along* these curves range up to 180 nm which is comparable to the lengths of MLs seen in the parallel sections [14]. These are consistent with the maximum dimensions of platelets measured using SAXS [2].

Just as in the parallel sections, the MLs in the perpendicular views occur in stacks of 3 or more plates both wrapping around the fibrils and as plates with larger radii of curvature further from fibrils. Stacks of up to 20 or more straight (flat) plates occurring between fibrils have been noted.

Rosettes

A striking visual feature of the mosaic of images from the perpendicular section is the presence of circular structures (Fig. 6a) with average radii of about 1 μm. These "rosettes" are cross-sections of clusters of collagen fibrils around a weakly defined central region which in a few instances consists of a dense, swirling patch of disordered MLs seemingly lacking in collagen fibrils. This μm-scale bunching of fibrils into a roughly cylindrical structure is reminiscent of the "rods" described in [28] as a feature of the demineralized bone sections studied by them using FIB-SEM serial sections. However, these rods were described to be 2–3 μm in diameter which is approximately double the diameter of the rosettes. Additional images of the rosettes are available in the Supplementary Fig. S2.

Osteonal Lamellae

The size of the area covered by the perpendicular section is such that we would expect to encounter the boundaries between two or more osteonal lamellae with different internal orientation of collagen fibrils [23]. In fact, we see what appear to be five discrete lamellae (Fig. 5) which cross the section at a steep angle. The thickness of the successive lamellae is not uniform: their thicknesses are ~ 4.9, 3.2, 5.5, and 3.4 μm. Only a small part of the fifth lamella is visible. Boundaries between lamellae are sharp, and approximately planar. In the thinner lamellae, collagen fibrils and MLs appear to be approximately parallel to the plane of the section and to the boundaries between the lamellae. The gap/overlap zone characteristic banding which reveals the presence of collagen fibrils is poorly defined and actually invisible over much of the area of these lamellae, potentially due to sample thickness. In the three wider lamellae, fibrils are seen in cross-section, and are clearly defined.

Comparing this appearance with images proposed for the twisted plywood structure [23], we see that rather than a continuous change in the angle of the fibrils from one lamella to the next, there is an abrupt change in orientation at each interlamellar boundary. This resembles to the "unidirectional" array described in [22] rather than the "fanning" array in which the orientation of the fibrils changes gradually. Because we have only one section through this sample, we cannot tell what is the angular offset of fibril orientation between adjacent osteonal lamellae; it could be quite variable [30]. The pattern of adjacent lamellae shown in Fig. 5 resembles the appearance of Fig. 10 of Reference [22] showing a section of demineralized, stained bone.

Note that the material viewed in the parallel section (discussed earlier) appears to have been confined to within a single osteonal lamella. There is no evidence that the section crossed a boundary between two adjacent lamellae, which would have resulted in an abrupt change in the orientation of the fibrils.

As in previous bright-field views (e.g., Fig. 6 in [15]), the HAADF-STEM images show that many of the circular features which we interpret as cross-sections of fibrils appear to be empty. This is either a result of preferential erosion by the Ga^+ ions used to produce the FIB section, or the much lighter contrast of carbon compared to mineral in HAADF-STEM imaging. To confirm that the black circular features are indeed collagen fibrils, one would expect that viewing them from 90° would show the characteristic collagen banding pattern. By using electron tomography on this perpendicular (transverse) section, we can clearly see the change from characteristic fibrillar structures with banding patterns like a parallel cut section, to the circular features viewed at 0° tilt. The full video showing this transition is available in Supplementary Video 1, while the individual screenshots that demonstrate this are shown in Fig. 7.
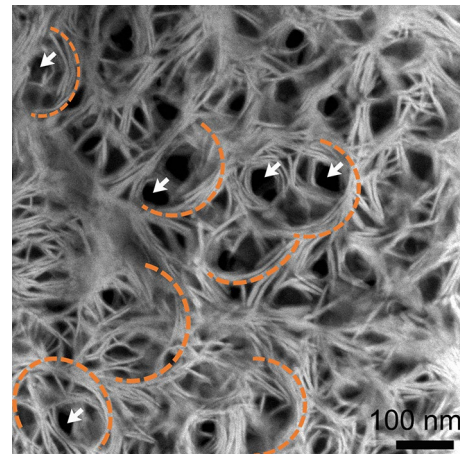
Fig. 8 HAADF-STEM image showing curvature of mineral lamellae on varying scales. Arrowheads mark single collagen fibrils with tightly wrapped stacks of MLs surrounding them, while stacks of MLs with larger radii of curvature (outlined in orange dotted lines) create higher level curvatures. These are composed of ML with less curvature because of their proximity to the fibril
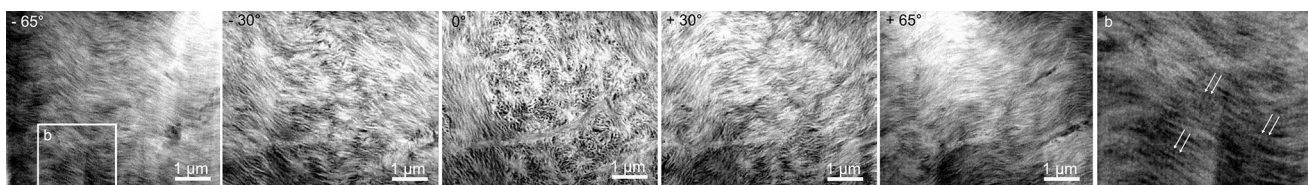
Fig. 7 HAADF-STEM images captured during an electron tomography tilt-series covering nearly ± 65°. From left to right, the tilt angles range from − 65° through 0° to + 65°. The dark-circular features visible at 0° tilt, which we believe to be collagen fibrils, clearly morph into collagen fibril patterns when viewed at high tilt (either fair right or far left images); the inset shows gap zones in the fibrils viewed at high angle with arrows to indicate three regions where collagen banding is particularly visible (collagen fibrils appear to run from bottom right to mid-left of inset). For more details, watch video S1

Discussion

Significance of the Curved Mineral Lamellae

Recently, we have shown that a model of bone in which the mineral is in the form of cylindrical, concentric plates surrounding a collagen fibril results in greater strength for the composite material than when the mineral is situated inside the fibril [15]. We comment in that paper that "From a structural mechanics perspective a hollow geometry gives stronger and stiffer response in bending and torsion, for the same bone tissue volume" [15]. Presumably, this same principle would also apply to larger-scale curved structures such as those which we observe here in cross-section (Fig. 8), with radii of curvature ranging to > 100 nm. Like the hemi-cylindrical lamellae immediately surrounding the fibrils, these larger structures are also composed of stacks of two or more MLs cemented together, which would confer even greater strength on the resulting structures. The overall pattern seen in the perpendicular section is one of smaller diameter curved features nested inside of curved sheets with larger radii of curvature.

In typical hierarchical fashion, this design feature is echoed at higher scales: the alternating concentric osteonal lamellae surrounding Haversian canals and the hollow shafts of long bones. The function of these larger-scale features is undoubtedly more complex than simply to add strength to the bone (e.g., it also provides sites for hematopoietic cells inside the hollow shafts). Furthermore, we cannot take for granted what would be the effect of these design features on the mechanical behavior of the composite material. This would require more formal modeling by finite-element analysis [15] or using continuum material analysis [7]. In addition, we note that even higher-order structural elements are suggested by structures such as the ~ 200-nm-diameter cylindrical stacks of MLs surrounding multiple collagen fibrils seen in Figs. 6 and 8. These could represent a higher hierarchical level of organization of bone which would also contribute to its strength.

Polycrystalline Structure and Curvature of MLs

The mineral of bone is apatite, a largely ionic-bonded structure. Under anisotropic stress, single crystals of apatite exhibit brittle fracturing, and would not be able to sustain a strain of more than 1–2% [31]. Therefore, the curvature of the plates which we observe here at various scales cannot be achieved by bending of single crystals of apatite. Using dark-field imaging of ion-milled sections of bone, we have previously demonstrated the polycrystalline structure of mineral lamellae [11, 32]. The curvature of the MLs either around collagen fibrils or in the space between them could be accommodated if the lattice planes of single crystals were slightly tilted with respect to the plane of adjacent crystals in order to generate the curved form of the lamella. Figure 9 shows a high-resolution transmission electron microscopy (HRTEM) of one of the curved lamellae surrounding a collagen fibril. It is clear that the planes in one set of crystals are slightly rotated with respect to the lattice planes of the neighboring crystals. This allows the complete lamella to curve around the fibril without requiring any bending of the crystals themselves.

Dimensions of Mineral Lamellae

As previously shown, MLs are plate-like structures which can only be clearly visualized when viewed edge-on [11, 14]. The thickness of individual MLs viewed in the parallel section is 5.6 ± 0.8 nm ($n = 20$), while in the perpendicular sections, the mineral lamellae surrounding the fibrils have an average thickness of 4.4 ± 0.7 nm, not significantly different. Their small variability in apparent thickness confirms that MLs whose planes are inclined by more than a few degrees are invisible in the HAADF images. Tilting of the plates with respect to the plane of the section would otherwise lead to larger projected areas for these edge-on views, so that the apparent projected thickness would be equal to $d*\sin\theta$ where θ is the angle between the plane of the ML and the section, and d is the width of an ML. The distribution of thicknesses is slightly skewed to lower values contrary to what would be expected if this effect were prevalent.
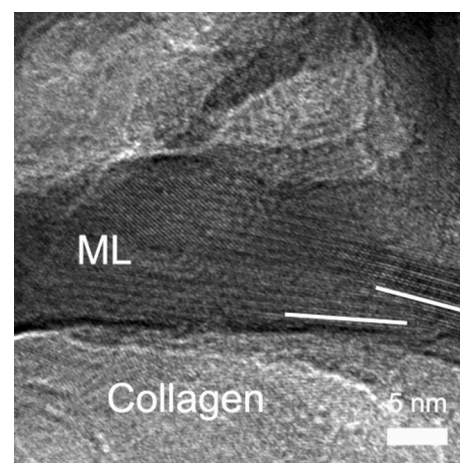
Fig. 9 HRTEM image of a single mineral lamella curving around collagen fibril (as in Fig. 8); lattice planes of adjacent crystals are tilted by a few degrees (white lines) to accommodate the bending of the lamella around the fibril. (from unpublished research by Luo, Binkley, Grandfield and Schwarcz). Scale = 5 nm

The average length of discrete isolated MLs in the parallel images is 160 ± 70 nm. Individual MLs can be traced in the parallel section for distances up to 300 nm but it is difficult to determine their maximum length because a single ML cannot be traced continuously through the stacks of multiple parallel MLs. The third dimension of the MLs (width) can be estimated where they are seen curling around fibrils (Fig. 6). The arc lengths of the MLs wrapping around fibrils are 50–80 nm which should correspond to the width of the MLs. The average length of curved MLs not spatially associated with a fibril is 80 ± 30 nm ($n = 16$). Combining that dimension with the lengths seen in parallel sections, we infer that, on average, the MLs are only slightly elongated in the direction parallel to the fibrils. We have, of course, no notion of what their plan view would be (elliptical, irregular, ragged?).

MLs Inside Fibrils

In sections of long bones cut perpendicular to the long axis of the bone (Fig. 6c), more than a third of the fibrils show MLs passing through their interior. It is possible that these MLs inside the fibrils may be an artifact produced during FIB milling. For example, the inside surfaces of curved plates at the edge of the fibril might be under tension and would curl more tightly when collagen is eroded by Ga^+ ions. However, low ion beam energy was used during the preparation of the sample, and most of the plates inside fibrils are straight and show no sign of increased curvature. It appears that they were formed inside of the fibril during the mineralization of the osteoid precursor of bone. Most of them are extensions of plates that also lie outside the fibril, and have the same thickness as MLs that surround the fibril. While this truly exemplifies "intrafibrillar mineralization," this is clearly not in the sense generally claimed by earlier researchers [5, 8] because the plates inside the fibrils are not restricted to gap zones, and partly extend outside the fibrils. It is well known that some of the mineral of bone occurs inside the fibrils, localized in the gaps between the C and N termini of collinear collagen molecules which are themselves aligned as 40-nm-wide zones spaced every 67 nm along the fibril. This mode of intrafibrillar mineralization is, however, clearly distinguishable from what we are observing here for the following reasons: (a) the MLs in question are not, as far as we can detect, limited to the 40-nm-wide gap zone but rather occur sporadically in some but not all of the fibrils; (b) the form of these MLs inside fibrils is clearly different from that of the mineralization in the gap zone; for example, in Fig. 4a, b we can see the relatively high-density (brighter) stacks of MLs (oriented parallel to the fibrils) contrasted against the fainter, less mineralized gap zones. Nevertheless, we could in principle denote these MLs

as intrafibrillar, but in a distinct sense from the usual gap zone mineral.

Development of the Ultrastructure of Bone

As we acquire more information about the formal characteristics of fully mineralized bone, we must also consider the processes by which this structure formed. While discussion of the details of this process is outside the goals of this paper, it is useful to note some constraints on this process which must be considered in any future attempt to model the genesis of bone.

It is widely understood that osteogenesis begins with the formation of a collagen scaffold consisting of a dense assemblage of fibrils in the form of osteoid [33]. Thus, it has been long understood that the form and possibly the protein structure of the fibril establishes the orientation and form of the first-formed mineralized structures. However, the next layers of added mineral are no longer in contact with collagen and presumably acquire their orientation guided by their proximity to the first generation of mineral lamellae. This process of addition of fibril-concentric layers must finally end as additional MLs are formed at distances of tens of nanometers from the surface of the fibril (Fig. 6b). At this point, the form of these additional mineral lamellae can no longer be determined by their conformity to the cylindrical form of the fibrils, especially as their radii of curvature are much larger than that of the fibrils. Therefore, some other, as yet unknown, form-defining factors must be acting to induce the curvature of some of the next generation of mineral lamellae. Finally, at positions more or less equidistant from neighboring fibrils, stacks of essentially flat, straight mineral lamellae are formed, completing the process of mineralization. In the course of this process, the centers of the fibrils have been gradually displaced away from each other by the added interfibrillar mineral lamellae. The final distance between centers of fibrils is 92 ± 28 nm, ranging from 60 to 130 nm, that is, between one and two fibril diameters. The initial co-registration of gap/overlap zones is not, however, disturbed during this process.

Presumably, this process takes place at distances from the surface of the adjacent osteoblast ranging from zero to some tens of nanometers since the mineralization process occurs over many hours to days subsequent to formation of the osteoid, while the osteoblast continues to lay down further osteoidal collagen [34].

As noted earlier, about 10–15% of the volume of the bone is composed of disordered material. Presumably, the scaffold which was mineralized to generate this material was a disordered (randomly oriented) region of collagen fibrils, similar to the collagen fibrils present in the disordered regions seen in [28]. Thus, the disordered character of these regions was

inherited from the initial collagen assembly process and is not due to anomalous mineralization processes.

Conclusions

Construction of large-scale (tens of μm^2) composite images of orthogonal sections of cortical bone has afforded us novel insights into its ultrastructural organization, formation, and mechanical integrity. We have observed several features not previously recognized in bone, most notably: (1) a super-structure of rosette-like clusters surrounded by mineral lamellae with chaotic fibril-free mineral lamellae inside of each rosette, (2) the presence of a hierarchical set of curved mineral lamellae, in addition to those already known to surround the fibrils, which may contribute to strengthening the bone matrix, (3) a clearer definition of the alternation of osteonal lamellae showing abrupt, rather than gradational, change in the orientation of mineral lamellae and associated fibrils at their interfaces. None of these features would have been recognizable in the previous generation of bright-field images.

This paper also confirms previous studies [11] showing that the appearance of bone in sections cut using ion milling methods reveals structures that were not detectable in microtome-cut sections. In particular, the present work shows that the same volume of a long bone viewed in a section parallel to the long axis of the bone is strikingly different in appearance from a section cut perpendicular to that axis. The latter sections invariably display an open mesh-work of cross-sections of fibrils surrounded by enveloping polycrystalline plates of apatite. Contrary to a statement in a recent paper by Shahar and Weiner [35], this pattern is not "…confined to localized areas outside… ordered material" but is rather present everywhere in a section cut in the appropriate orientation.

The present study allows us to see how the nanometer-scale features of the mineralized collagen scaffold, previously observed only at the scale of tens of nm, can be extended to a μm-scale and, by extension, over the entire volume of bone. The higher resolution and compositional contrast of the HAADF images in this paper clarifies many of the details of this nanometer-scale structure which will eventually lead to a better understanding of how bone is formed.

Author Contributions K.G. and H.P.S designed the experiments. V.V. and K.G. performed electron microscopy. All authors analyzed the data. K.G. and H.P.S prepared the manuscript with contributions, revisions, and figure preparation from V.V.

Compliance with Ethical Standards

References

1. Orgel JPRO, Irving TC, Miller A, Wess TJ (2006) Microfibrillar structure of type I collagen in situ. Proc Natl Acad Sci 103:9001–9005. https://doi.org/10.1073/pnas.0502718103
2. Rinnerthaler S, Roschger P, Jakob HF et al (1999) Scanning small angle X-ray scattering analysis of human bone sections. Calcif Tissue Int 64:422–429. https://doi.org/10.1007/PL00005824
3. Weiner S, Price PA (1986) Disaggregation of bone into crystals. Calcif Tissue Int 39:365–375. https://doi.org/10.1007/BF02555173
4. Kim H-M, Rey C, Glimcher MJ (1995) Isolation of calcium-phosphate crystals of bone by non-aqueous methods at low temperature. J Bone Miner Res 10:1589–1601. https://doi.org/10.1002/jbmr.5650101021
5. Landis WJ, Song MJ, Leith A et al (1993) Mineral and organic matrix interaction in normally calcifying tendon visualized in three dimensions by high-voltage electron microscopic tomography and graphic image reconstruction. J Struct Biol 110:39–54
6. Siperko LM, Landis WJ (2001) Aspects of mineral structure in normally calcifying avian tendon. J Struct Biol 135:313–320. https://doi.org/10.1006/jsbi.2001.4414
7. Hamed E, Novitskaya E, Li J et al (2012) Elastic moduli of untreated, demineralized and deproteinized cortical bone: validation of a theoretical model of bone as an interpenetrating composite material. Acta Biomater 8:1080–1092. https://doi.org/10.1016/j.actbio.2011.11.010
8. Alexander B, Daulton TL, Genin GM et al (2012) The nanometre-scale physiology of bone: steric modelling and scanning transmission electron microscopy of collagen-mineral structure. J R Soc Interface 9:1774–1786
9. Su X, Sun K, Cui FZ, Landis WJ (2003) Organization of apatite crystals in human woven bone. Bone 32:150–162
10. Lees S, Prostak K (1988) The locus of mineral crystallites in bone. Connect Tissue Res 18:41–54. https://doi.org/10.3109/03008208809019071
11. McNally EA, Schwarcz HP, Botton GA, Arsenault AL (2012) A model for the ultrastructure of bone based on electron microscopy of ion-milled sections. PLoS ONE. https://doi.org/10.1371/journal.pone.0029258
12. Fratzl P, Gupta HS, Paschalis EP, Roschger P (2004) Structure and mechanical quality of the collagen–mineral nano-composite

in bone. J Mater Chem 14:2115–2123. https://doi.org/10.1039/B402005G

13. Fratzl P, Gupta HS, Paris O et al (2005) Diffracting "stacks of cards"—some thoughts about small-angle scattering from bone. Prog Colloid Polym Sci 130:33–39. https://doi.org/10.1007/b107343

14. Schwarcz HP (2015) The ultrastructure of bone as revealed in electron microscopy of ion-milled sections. Semin Cell Dev Biol 46:44–50

15. Schwarcz HP, Abueidda D, Jasiuk I (2017) The ultrastructure of bone and its relevance to mechanical properties. Front Phys. https://doi.org/10.3389/fphy.2017.00039

16. Benezra Rosen V, Hobbs LW, Spector M (2002) The ultrastructure of anorganic bovine bone and selected synthetic hyroxyapatites used as bone graft substitute materials. Biomaterials 23:921–928. https://doi.org/10.1016/S0142-9612(01)00204-6

17. Nalla RK, Porter AE, Daraio C et al (2005) Ultrastructural examination of dentin using focused ion-beam cross-sectioning and transmission electron microscopy. Micron 36:672–680

18. Jantou-Morris V, Horton MA, McComb DW (2010) The nanomorphological relationships between apatite crystals and collagen fibrils in ivory dentine. Biomaterials 31:5275–5286. https://doi.org/10.1016/j.biomaterials.2010.03.025

19. Langelier B, Wang X, Grandfield K (2017) Atomic scale chemical tomography of human bone. Sci Rep 7:39958

20. Grandfield K, Engqvist H (2012) Focused ion beam in the study of biomaterials and biological matter. Adv Mater Sci Eng 2012:1–6

21. Grandfield K (2015) Bone, implants, and their interfaces. Phys Today 68:40–45. https://doi.org/10.1063/PT.3.2748

22. Reznikov N, Shahar R, Weiner S (2014) Bone hierarchical structure in 3 dimensions. Acta Biomater 10:3815–3826. https://doi.org/10.1016/j.actbio.2014.05.024

23. Giraud-Guille MM (1988) Twisted plywood architecture of collagen fibrils in human compact bone osteons. Calcif Tissue Int 42:167–180. https://doi.org/10.1007/BF02556330

24. Schindelin J, Arganda-Carreras I, Frise E et al (2012) Fiji: an open-source platform for biological-image analysis. Nat Methods 9:676–682. https://doi.org/10.1038/nmeth.2019

25. Weiner S, Wagner HD (1998) The material bone: structure-mechanical function relations. Annu Rev Mater Sci 28:271–298. https://doi.org/10.1146/annurev.matsci.28.1.271

26. Raspanti M, Viola M, Forlino A et al (2008) Glycosaminoglycans show a specific periodic interaction with type I collagen fibrils. J Struct Biol 164:134–139. https://doi.org/10.1016/j.jsb.2008.07.001

27. Orgel JPRO, Eid A, Antipova O et al (2009) Decorin core protein (decoron) shape complements collagen fibril surface structure and mediates its binding. PLoS ONE 4:e7028

28. Reznikov N, Shahar R, Weiner S (2014) Three-dimensional structure of human lamellar bone: the presence of two different materials and new insights into the hierarchical organization. Bone 59:93–104

29. Reznikov N, Almany-Magal R, Shahar R, Weiner S (2013) Three-dimensional imaging of collagen fibril organization in rat circumferential lamellar bone using a dual beam electron microscope reveals ordered and disordered sub-lamellar structures. Bone 52:676–683

30. Gebhardt W (1906) Ueber funktionell wichtige Anordnungsweisen der groberen und feineren Bauelemente des Wirbeltierknochens. Arch Entw Mech 20:187–322

31. Katz JLL, Ukraincik K (1971) On the anisotropic elastic properties of hydroxyapatite. J Biomech 4:221–227. https://doi.org/10.1016/0021-9290(71)90007-8

32. Schwarcz HP, McNally EA, Botton GA (2014) Dark-field transmission electron microscopy of cortical bone reveals details of extrafibrillar crystals. J Struct Biol 188:240–248. https://doi.org/10.1016/j.jsb.2014.10.005

33. McKee MD, Cole WG (2012) Bone matrix and mineralization. In: Pediatric bone. pp 9–37

34. Roschger P, Paschalis EP, Fratzl P, Klaushofer K (2008) Bone mineralization density distribution in health and disease. Bone 42:456–466. https://doi.org/10.1016/j.bone.2007.10.021

35. Shahar R, Weiner S (2017) Open questions on the 3D structures of collagen containing vertebrate mineralized tissues: A perspective. J Struct Biol https://doi.org/10.1016/j.jsb.2017.11.008